

# Superconductivity in metallic hydrogen

D. van der Marel<sup>1,\*</sup> and C. Berthod<sup>1</sup>

<sup>1</sup>*Department of Quantum Matter Physics, University of Geneva,  
24 Quai Ernest-Ansermet, 1211 Geneva 4, Switzerland*

(Dated: June 28, 2024)

Superconductivity, the amazing phenomenon of lossless transmission of electric current through metallic wires, requires cooling of the wire to low temperatures. Metallic hydrogen is considered as the most likely candidate for superconductivity at very high temperatures, possibly even room temperature. However, as a result of various approximations used, conflicting theoretical predictions exist for the range of temperatures where superconductivity is expected to occur. Here we avoid those approximations and confirm that metallic hydrogen is indeed a superconductor, but this is limited to temperatures far below previous estimates. We exploit the “jellium” model proposed in 1966 by De Gennes, where superconductivity is caused by the combination of Coulomb repulsion between the electrons and Coulomb attraction between the protons and the electrons. We find that the superconducting order develops over an energy range far exceeding the characteristic phonon energy, and that the phase of the order parameter flips 180 degrees at the characteristic phonon energy above and below the Fermi energy.

## INTRODUCTION

According to the theory of Bardeen Cooper and Schrieffer [1], superconductivity is caused by electron-phonon coupling, the coupling of the electrons to vibrations of the lattice. A pedagogical description of this mechanism was introduced by De Gennes using the “jellium model”, demonstrating that electron-phonon coupling can result in an effective interaction between electrons which overcomes the Coulomb repulsion between the electrons [2]. De Gennes indicated a number of restrictions for the range of applicability of the jellium model, notably that the model assumes the absence of core electrons. This limits the part of the periodic table where the model can be applied to hydrogen and helium, of which hydrogen is by far the most promising candidate. In 1968, Ashcroft suggested that the bulk of Jupiter is composed of hydrogen in the metallic state and that part of the bulk (with a temperature 100–200 K) may be in a superconducting state [3]. Various refinements were made in later papers using Eliashberg strong coupling theory [4–6], predicting superconductivity above 200 K. In 1981, Jaffe and Ashcroft pointed out the possibility that metallic hydrogen may be a superconducting liquid in the density range  $3.9 \times 10^{23} \text{ cm}^{-3} < n < 7.3 \times 10^{23} \text{ cm}^{-3}$ , with a maximum  $T_c \approx 141 \text{ K}$  for  $n = 6.4 \times 10^{23} \text{ cm}^{-3}$ . The possibility that pulsars are cold magnetic white dwarfs was discussed, also in 1968, by Ginzburg and Khirzhnits [7]. They pointed out that the superconductivity of a certain layer of the star may be an essential factor and derived a simple expression for  $T_c$  for light elements. Their expression for hydrogen, based on De Gennes’ jellium model, is reproduced in Eq. (A2). In a subsequent paper, Khirzhnits [8] published a slightly different version of this expression, which is reproduced in Eq. (A4).

In recent years, superconductivity in hydrogen-rich compounds has seen a revival, where numerical predictions and experimental confirmation of superconductivity near and above room temperature have entered the stage [9]—and to some extent left it again [10]. The calculation of  $T_c$  for a multi-element material is a complex task, and a certain degree of coarse-graining of the momentum dependence and energy dependence of the electron-phonon coupling and the screened Coulomb interaction is unavoidable.

The values of  $T_c$  that follow from Ginzburg and Khirzhnits’ expressions are displayed in Fig. 1. The fact that the results are so different may have to do with approximations beyond those of the jellium model, that were necessary in view of limitations of the computational resources available at that time. For this reason, and without pretence of addressing the pairing mechanism of the aforementioned more complex materials, we return to the model interaction proposed by De Gennes and explore its properties within the BCS formalism [1] without additional approximations.

## SUPERCONDUCTIVITY IN THE JELLIUM MODEL

Physically, a “jellium” would be realized if the material could be made dense enough, that not only the electrons but also the nuclei are in a liquid state. The formal requirement is that the Wigner-Seitz radius (radius of a sphere whose volume is equal to the volume per particle) of the electrons and that of the nuclei are both sufficiently small. For the case of hydrogen, this possibility was proposed—and its properties were explored—in a series of papers by Ashcroft and collaborators [15–18]. A recent review of the phases of highly compressed hydrogen up to 500 GPa (Carlo Pierleoni in Ref. [9]) does not address this proposal, but points out that the lack of experimen-

---

\* [dirk.vandermarel@unige.ch](mailto:dirk.vandermarel@unige.ch)

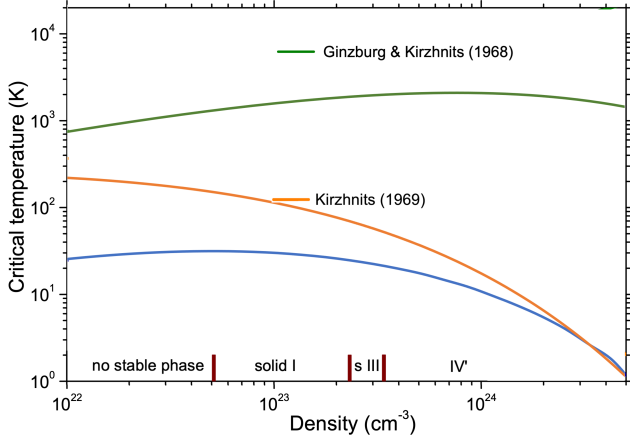


Figure 1. Superconducting transition temperature of metallic hydrogen. Comparison of three calculations of  $T_c$  in hydrogen at different densities, each of them using the jellium model [2]. Green curve: Ginzburg and Kirzhnits expression [7] reproduced in Eq. (A2). Orange curve: Kirzhnits' expression [8] reproduced in Eq. (A4). Blue curve: present result. The different phases indicated along the bottom axis refer to the zero-temperature limit. The labels “solid I” (solid, phase I) and “s III” (solid, phase III) and IV' are adapted from Fig. 3 of Ref. [11], where IV' is possibly a liquid phase [12]. To relate the pressure to the density, the data in Fig. 4 of Ref. [13] were used. In the region “no stable phase” the density is below that of solid molecular hydrogen in the limit of zero pressure [14].

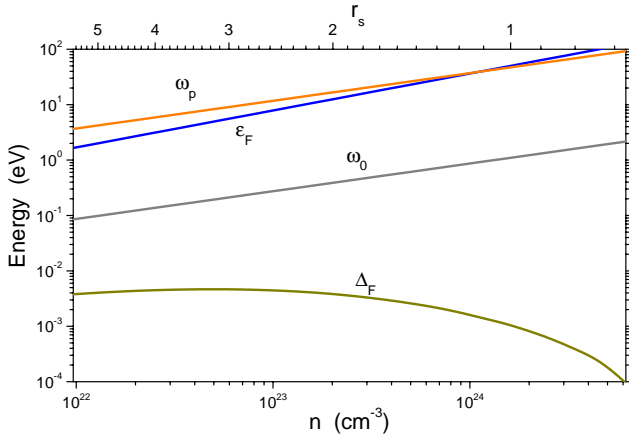


Figure 2. Relevant energy scales of metallic hydrogen as a function of density. The lower (upper) horizontal axis indicates the density (Wigner-Seitz radius).

tal information about the crystalline structure together with the large nuclear quantum effects for hydrogen poses a challenge to *ab initio* calculations. The jellium model is an interesting alternative approach since (i) crystallographic information is not required, (ii) the mathematics is relatively simple, (iii) it is optimally suited for hydrogen because the model assumes the absence of core electrons, and (iv) the model rests on only two parameters:

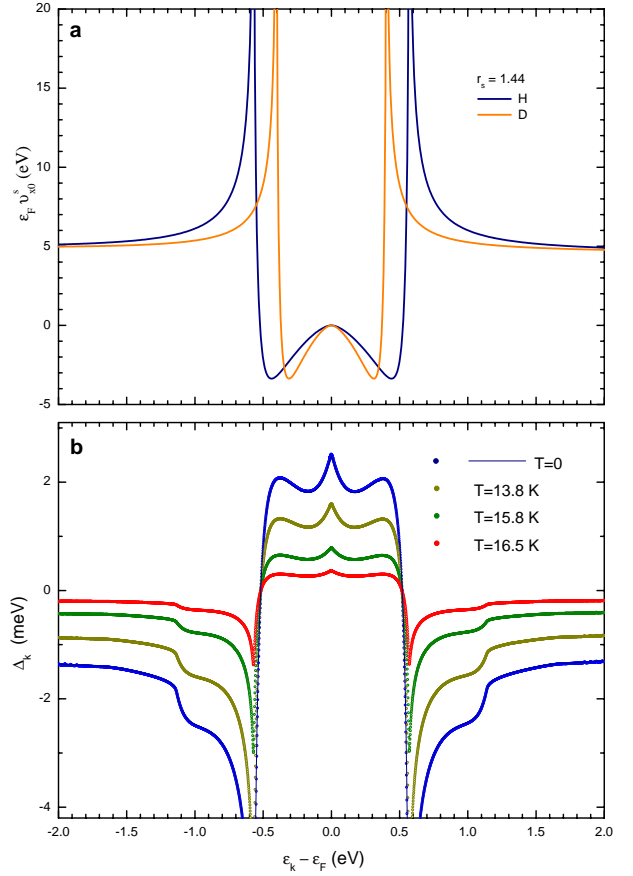


Figure 3. Energy dependence of the interaction and the gap function. **a**  $s$ -wave coupling function,  $\varepsilon_F v_{x,0}^s$ , as a function of energy  $\varepsilon_k = \varepsilon_F x$  in the case of hydrogen ( $m_N = m_p$ , blue) and deuterium ( $m_N = 2m_p$ , orange) with  $r_s = 1.44$ . **b** Energy dependence of the order parameter for  $r_s = 1.44$  in the case of hydrogen ( $m_N = m_p$ ), and for four temperatures below  $T_c$  ( $\sim 17$  K). For  $T = 0$  the results computed with two different numerical codes are compared. Open symbols: Numerical code where the integrals are calculated with the trapezoidal rule (Appendix C). Continuous curve: Numerical code where the integrals are calculated with a piecewise-continuous function of  $x$  (Appendix D). The difference of these two curves is given in Extended Data Fig. 1.

the Wigner-Seitz radius of the electrons and the mass of the nuclei.

At this point, it is useful to introduce the relevant energy scales of the system. In Fig. 2, the plasmon energy of the electrons  $\omega_p$ , the Fermi energy of the electrons  $\varepsilon_F$ , the plasmon energy of the nuclei  $\omega_0$ , and the gap energy at the Fermi surface  $\Delta_F$  (anticipating for the latter the discussion of the present manuscript) are displayed as a function of the electron density  $n$  and—the on the opposite axis—the Wigner-Seitz radius  $r_s = a_0^{-1}(4\pi n/3)^{-1/3}$ , where  $a_0 = 0.529177$  Å is the Bohr radius. For the density range relevant for metallic hydrogen ( $r_s \sim 1.5$ ) the plasma energy and the Fermi energy are of the same order

of magnitude, and for all densities  $\omega_p, \varepsilon_F \gg \omega_0 \gg \Delta_F$ . The Wigner-Seitz radius plays the role of the coupling constant [8], *i.e.*,  $\lambda \approx 0.16 r_s$  in  $T_c \propto e^{-1/\lambda}$  [see Eq. (A3)], so that for  $r_s \sim 1.5$  the coupling constant  $\sim 0.25$ , which is in the weak coupling regime. Furthermore, since  $\omega_0 \ll \varepsilon_F$ , the system is in the regime where the motion of the nuclear particles is slow compared to that of the electrons. All in all, this implies that for the density range of interest the BCS model [1] can be used. The coupling should be considered strong for  $r_s > 6$  and predictions with the BCS model become less reliable. Following De Gennes [2], we adopt as a starting point the Coulomb interaction screened by electrons and nuclear particles

$$V^{\text{eff}}(q, \omega) = \frac{4\pi e^2}{q^2} \frac{1}{\epsilon(q, \omega)}, \quad (1)$$

where  $\epsilon(q, \omega)$  is the dielectric function and  $\mathbf{q} = \mathbf{k} - \mathbf{p}$  represents the transferred momentum. We furthermore

$$\psi_x = - \int_0^\infty dy \sqrt{y} v_{x,y}^s \frac{\psi_y}{2\sqrt{(y-1)^2 + \psi_y^2}} \tanh\left(\frac{\sqrt{(y-1)^2 + \psi_y^2}}{2\tau}\right), \quad (3)$$

where

$$v_{x,y}^s = \frac{(x-y)^2}{2\sqrt{xy}[4z_0^2 - (x-y)^2\gamma^{-2}]} \ln \left| \frac{4(x-y)^2 - (\sqrt{x} - \sqrt{y})^2 [4z_0^2 - (x-y)^2\gamma^{-2}]}{4(x-y)^2 - (\sqrt{x} + \sqrt{y})^2 [4z_0^2 - (x-y)^2\gamma^{-2}]} \right| \quad (4)$$

is the interaction in the *s*-wave pairing channel, and is displayed in the top panel of Fig. 3. The two constants in this expression,

$$z_0^2 = \frac{4m_e}{3m_N}, \quad \gamma^2 = \left(\frac{4}{9\pi^4}\right)^{1/3} r_s, \quad (5)$$

depend uniquely on the nuclear mass  $m_N$  of the isotope (hydrogen or deuterium in the present context) and the Wigner-Seitz radius  $r_s$ . Remarkably, for zero energy shift ( $x = y$ ) the interaction is exactly zero. The interaction is furthermore negative for small energy shift, passes through a minimum, changes sign, passes through a positive logarithmic singularity and asymptotically approaches the Thomas-Fermi screened Coulomb repulsion at high energies. In the most common implementation of the theory of Bardeen Cooper and Schrieffer [1] the interaction is assumed to be constant and attractive in the interval  $\pm\omega_0$  around the Fermi energy, corresponding to an interaction at the Fermi level that is both non-zero and attractive. Given that in the present model the interaction at the Fermi energy is zero, it is not overwhelmingly obvious that such an interaction would induce the Cooper instability [19]. One of the motivations for the present study was to investigate whether the BCS variational wave function has a non-trivial solution with this interaction. To address this question, we solved the gap equation numerically (Appendix C) and calculated the gap function, the condensation energy (Eq. C11), and the specific heat (Eq. B13). Instead of substituting  $\hbar\omega = \varepsilon_k - \varepsilon_p$  in the interaction and solving the BCS gap equations, it is in principle possible to solve the Eliashberg equations and calculate  $T_c$  [20]. While the relevant set of equations for the present case could be identified without a problem, due to the simultaneous energy- and momentum dependence of the interaction, the numerical algorithm poses a computational challenge which we haven't been able to overcome yet.

adopt the procedure of De Gennes [2] and Kirzhnits [8], and substitute  $\hbar\omega = \varepsilon_k - \varepsilon_p$ . The argument, provided on pp. 100–102 of Ref. [2], is that with this substitution the effective interaction has exactly the form of the matrix element  $V_{k,p}$  between an initial state where two electrons are in the plane wave states  $|k, -k\rangle$  and a final state where the electrons are in  $|p, -p\rangle$ .

For a high-density electron gas, the dielectric function in the jellium approximation is described by

$$\epsilon(q, \omega) = 1 + \frac{k_0^2}{q^2} - \frac{\omega_0^2}{\omega^2}, \quad (2)$$

where  $k_0$  is the Thomas-Fermi screening wavevector and  $\omega_0$  is the plasma frequency of the positively charged nuclei. Expressing the electron energies and the gap energy in units of the Fermi energy, *i.e.*,  $\varepsilon_k = x\varepsilon_F$ ,  $\Delta_k = \psi_x\varepsilon_F$ , the gap equation obtains the following compact form (Appendix B)

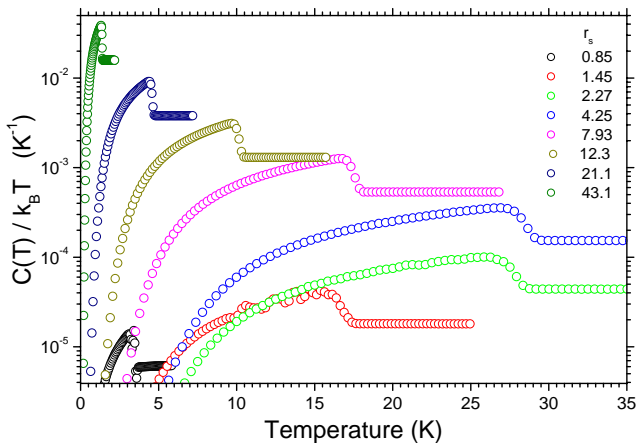


Figure 4. Specific heat divided by temperature for eight different values of  $r_s$  in the case of hydrogen ( $m_N = m_p$ ).

## RESULTS

The resulting gap function is shown in the lower panel of Fig. 3 for hydrogen assuming a Wigner-Seitz radius  $r_s = 1.44$  at four temperatures below  $T_c$ . We see that the gap function changes sign near the energy where  $v_{x,0}^s$  changes sign, and shows a negative peak (which is however not a singularity) near the energy where  $v_{x,0}^s$  has a log-singularity. One of the remarkable features is that the region of finite order parameter—and temperature evolution thereof—is not limited in any way to a narrow range around the Fermi energy. Although this doesn't contribute significantly to the free energy of the electrons, experimental probes such as photo-emission, optics and tunneling spectroscopy can in principle pick up the temperature dependency of the order parameter at energies far beyond the characteristic energy of the phonons that mediate the pairing interaction. Another feature—not visible on this scale—is that for large positive energy  $\Delta_k = \varepsilon_F \psi_x$  is proportional to  $1/x$ .

The temperature-dependent specific heat is shown in Fig. 4. The drop in the specific heat was used to determine  $T_c$ , shown in Fig. 5. The maximum is reached for  $r_s \sim 3$ , where in the case of hydrogen  $T_c \sim 30$  K. To obtain an accurate estimate of  $T_c$ , the gap equation has to be solved for many temperatures for each  $r_s$  value. Since this is a time-consuming calculation, we also tested a less cumbersome method, namely to use the following proxy for  $T_c$ :

$$T_c^* = A\sqrt{\varepsilon_F E_c}/k_B. \quad (6)$$

In the most commonly used implementation of BCS theory, the interaction is assumed constant between  $\pm\omega_0$  and zero elsewhere. In this case the condensation energy *per particle* is

$$E_c = \frac{3\Delta_0^2}{8\varepsilon_F} \quad (7)$$

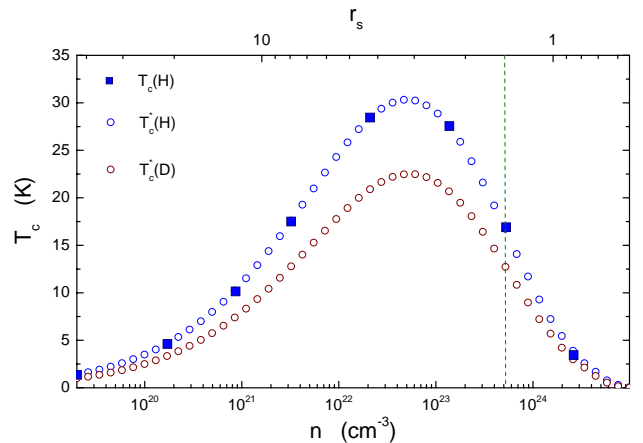


Figure 5. Superconducting transition temperature as a function of density. Square symbols:  $T_c$  for  $m_N = m_p$  (hydrogen) determined from the specific heat jump (Fig. 4). The vertical dashed line indicates the density of metallic hydrogen [21]. Open symbols: Effective  $T_c$  determined from the condensation energy [Eq. (6) with  $A = 0.925$ ] for hydrogen (blue) and deuterium (orange,  $m_N = 2m_p$ ).

and the gap over  $T_c$  ratio

$$\frac{2\Delta_0}{k_B T_c} = 3.53. \quad (8)$$

Combining these two expressions one obtains  $A = 0.925$ . The results for  $T_c$  and  $T_c^*$  are displayed in Fig. 5 for hydrogen (blue symbols) and deuterium (orange symbols). The density dependence of  $T_c^*$ , shown in Fig. 5, is described by a dome. We also see that the mass-dependence of  $T_c^*$  follows closely the conventional isotope effect, *i.e.*, the ratio  $T_c^*(\text{H})/T_c^*(\text{D}) \sim \sqrt{2}$ . The result for hydrogen is also displayed as the dark blue curve in Fig. 1.

Ashcroft estimated  $T_c \sim 200$  K for dense hydrogen [3, 4] assuming a coupling constant  $\lambda \approx 1.5$ . The  $T_c$  values obtained with the jellium model are an order of magnitude below these estimates as a result of the relatively low coupling constant which for  $r_s \sim 1.5$ , using Kirzhnits' expression [see Eq. (A3)], hovers around  $\lambda \sim 0.25$ . A natural question is what the value of  $T_c$  would become if, instead of using the jellium approximation, the full potential of the positively charged nuclear particles would be taken into account. Since no structural information is available for densities corresponding to the metallic phase of hydrogen, it is not possible at the present stage to predict the superconducting properties for the actual atomic configuration of solid or liquid metallic hydrogen beyond the jellium approximation. However, based on what is known for the alkali metals, it is reasonable to postulate that the Fermi surface would be entirely contained within the first Brillouin zone and that the energy-momentum dispersion of the electrons is to a good approximation described by the effective mass formalism. While such a modification of the band structure would change the

$r_s$  value for any given density, the upper limit for  $T_c(r_s)$  would remain 30 K.

Hirsch [22] has argued on the basis of Alfvén’s theorem [23] that for the Meissner effect to occur it is essential that the charge carriers have *negative* effective mass; otherwise the transition would not be reversible. On the one hand we have demonstrated in the present study that, with De Gennes’ effective electron-electron interaction, the BCS variational wave-function of free electrons—which have a positive mass—has a non-trivial ground state with a finite order parameter. On the other hand, according to Hirsch’s argument there can be no Meissner effect in this model in view of the positive mass. If this argument is correct, this would imply that interacting electrons *can* condense into a state with a BCS-type order parameter but, in view of the positive mass of the electrons this state of matter differs in a fundamental way from a superconductor and does not have a Meissner effect. We nonetheless continue to use the terminology of superconductivity for the remainder of the discussion and return to the questions about superconductivity in white dwarf stars and in the interior of Jupiter mentioned in the introduction. To begin with the latter, the black-body temperature provides a lower limit of the temperature of a planet, which in the case of Jupiter is 109.9 K [24]. For white dwarfs the situation is more complicated. For the coldest one that has been observed an upper limit of 3000 K was estimated [25]. This does not exclude that

the temperature is lower than 30 K, however, given the current age of the known universe it is unlikely that sufficient time has elapsed for a white dwarf to cool down to such a low temperature. All in all it seems unlikely both for the case of Jupiter or for white dwarfs that the temperature is low enough (lower than 30 K) to contain metallic hydrogen in the superconducting state.

## CONCLUSIONS

The superconducting pairing in metallic hydrogen involves an intricate interplay of the Coulomb repulsion between the electrons and an attractive phonon-mediated pairing mechanism. One of the consequences is that the superconducting order parameter has a  $180^\circ$  phase shift at the characteristic energy of the phonons. The outcome for the superconducting critical temperature ( $T_c < 30$  K) is much lower than the  $T_c$  predicted in Refs. [3–6] and previous results using the same model [7, 8]. For energies far above the phonon energy range, the amplitude of the order parameter is of the same order of magnitude as that at the Fermi surface.

## ACKNOWLEDGEMENTS

We gratefully acknowledge valuable discussions with Peter Hirschfeld and Louk Rademaker.

### Appendix A: Previous expressions for $T_c$ using the jellium model

Ginzburg and Kirzhnits [7] used the following expressions

$$T_c = \hbar\omega_0 \exp\left(-\frac{1}{NV}\right) \quad \text{with} \quad NV = \frac{e^2}{\hbar v_F} = \left(\frac{4}{9\pi}\right)^{1/3} r_s \quad \text{and} \quad \omega_0^2 = \frac{4\pi n e^2}{m_p}. \quad (\text{A1})$$

The combination of these expressions gives

$$k_B T_c = \text{Hr} \sqrt{\frac{3m_e}{m_N}} \frac{1}{r_s^{3/2}} \exp\left[-\left(\frac{9\pi}{4}\right)^{1/3} \frac{1}{r_s}\right]. \quad (\text{A2})$$

where  $\text{Hr} \approx 27$  eV is the Hartree energy. Kirzhnits [8] used

$$\Delta = \alpha\omega_0 \exp\left(-\frac{8}{\pi^2\alpha}\right) \quad \text{with} \quad \alpha = \frac{e^2}{\pi v_F} = \left(\frac{4}{9\pi^4}\right)^{1/3} r_s \quad (\text{A3})$$

and the same definition of  $\omega_0$ , stating that the critical temperature  $T_c$  is connected with this quantity in the usual manner. Combining these expressions gives

$$k_B T_c = \text{Hr} \frac{e^\gamma}{\pi} \left(\frac{2}{3\pi^2}\right)^{2/3} \sqrt{\frac{3m_e}{m_N}} \frac{1}{r_s^{1/2}} \exp\left[-2\left(\frac{12}{\pi}\right)^{2/3} \frac{1}{r_s}\right] \quad (\text{A4})$$

where  $\gamma \approx 0.577$  is the Euler constant.

## Appendix B: The gap equation

If the BCS variational wave function is applied to a system of band electrons with energy-momentum dispersion  $\epsilon_k$  and an electron-electron interaction  $V_{\mathbf{k},\mathbf{p}}^{\text{eff}}$ , one obtains the following expression for the grand potential [26]

$$\Omega = \sum_{\mathbf{k}} \left[ -2k_{\text{B}}T \ln \left( 1 + e^{-E_k/k_{\text{B}}T} \right) + \xi_k - E_k + \frac{|\Delta_k|^2}{E_k} \tanh \left( \frac{E_k}{2k_{\text{B}}T} \right) \right] + \sum_{\mathbf{k},\mathbf{p}} \frac{\Delta_k \Delta_p^* V_{\mathbf{k},\mathbf{p}}^{\text{eff}}}{4E_k E_p \nu} \tanh \left( \frac{E_p}{2k_{\text{B}}T} \right) \quad (\text{B1})$$

where  $\xi_k = \epsilon_k - \mu$ ,  $\mu$  is the chemical potential, and  $E_k = \sqrt{\xi_k^2 + |\Delta_k|^2}$ . In equilibrium, where  $\Delta_k$  corresponds to the set of values that minimizes  $\Omega$ , the number of electrons follows from the relation

$$N = -\frac{\partial \Omega}{\partial \mu} = \sum_{\mathbf{k}} \left[ 1 - \frac{\xi_k}{E_k} \tanh \left( \frac{E_k}{2k_{\text{B}}T} \right) \right] \quad (\text{B2})$$

We reserve the symbols  $N_0$  for the number of electrons,  $n_0$  for the electron density and  $\varepsilon_{\text{F}}$  for the chemical potential at  $T = 0$  and in the absence of superconducting order.  $V_{\mathbf{k},\mathbf{p}}^{\text{eff}}$  represents the effective interaction between the electrons. Here we consider the screened Coulomb interaction [2]

$$V^{\text{eff}}(q, \omega) = \frac{4\pi e^2}{q^2} \frac{1}{\epsilon(q, \omega)} \quad (\text{B3})$$

For  $\epsilon(q, \omega)$  we adopt the the jellium model:

$$\epsilon(q, \omega) = 1 + \frac{k_0^2}{q^2} - \frac{\omega_0^2}{\omega^2} \quad (\text{B4})$$

where

$$k_0^2 = \frac{4e^2 m_e k_{\text{F}}}{\pi \hbar^2}, \quad \omega_0^2 = \frac{4\pi n e^2}{m_N} \quad (\text{B5})$$

so that

$$V^{\text{eff}}(q, \omega) = \frac{4\pi e^2 \omega^2}{k_0^2 \omega^2 + (\omega^2 - \omega_0^2) q^2} \quad (\text{B6})$$

To obtain a more compact formulation we multiply both sides of Eq. (B1) with  $1/(N_0 \varepsilon_{\text{F}}) = 3\pi^2/(\nu k_{\text{F}}^3 \varepsilon_{\text{F}})$ , divide the electron energies by the Fermi energy and adopt Ashcroft's notation [6]  $\gamma$  for the Thomas-Fermi factor. Concretely we define the following set of dimensionless quantities

$$\begin{aligned} w &= \frac{\Omega}{N_0 \varepsilon_{\text{F}}}, & x &= \frac{\varepsilon_k}{\varepsilon_{\text{F}}}, & y &= \frac{\varepsilon_p}{\varepsilon_{\text{F}}}, & z &= x - y = \frac{\hbar \omega}{\varepsilon_{\text{F}}} \\ \psi_x &= \frac{\Delta_k}{\varepsilon_{\text{F}}}, & \tau &= \frac{k_{\text{B}}T}{\varepsilon_{\text{F}}}, & z_0 &= \sqrt{\frac{4m_e}{3m_N}}, & \gamma &= \frac{k_0}{2k_{\text{F}}} = \left( \frac{2}{3\pi^2} \right)^{1/3} \sqrt{r_s}. \end{aligned} \quad (\text{B7})$$

Since  $\psi_k$  is isotropic for the s-wave pairing assumed here,  $V_{\mathbf{k},\mathbf{p}}^{\text{eff}}$  is the only term in the free-energy expression that depends on the angular coordinates of  $\mathbf{k}$  and  $\mathbf{p}$ , and only on the relative angle of these two. This way we obtain

$$\begin{aligned} w &= \frac{3}{4} \int_0^\infty dx \sqrt{x} \left[ -2\tau \ln \left( 1 + e^{-E_x/\tau} \right) + \xi_x - E_x + \frac{|\psi_x|^2}{E_x} \tanh \left( \frac{E_x}{2\tau} \right) \right] + \\ &+ \frac{3}{4} \int_0^\infty dx \sqrt{x} \int_0^\infty dy \sqrt{y} \frac{\psi_x \psi_y^* v_{x,y}^s}{4E_x E_y} \tanh \left( \frac{E_x}{2\tau} \right) \tanh \left( \frac{E_y}{2\tau} \right), \end{aligned} \quad (\text{B8})$$

where  $\xi_x = x - \mu/\varepsilon_{\text{F}}$ ,  $E_x = \sqrt{\xi_x^2 + |\psi_x|^2}$  and

$$v_{x,y}^s = \frac{z^2}{2\sqrt{xy}[4z_0^2 - z^2\gamma^{-2}]} \ln \left| \frac{4z^2 - (\sqrt{x} - \sqrt{y})^2 [4z_0^2 - z^2\gamma^{-2}]}{4z^2 - (\sqrt{x} + \sqrt{y})^2 [4z_0^2 - z^2\gamma^{-2}]} \right| \quad (\text{B9})$$

is the interaction in the  $s$ -wave pairing channel. The equilibrium condition

$$\forall x : \quad \frac{\partial w}{\partial \psi_x} = 0 \quad (\text{B10})$$

results in the gap equation

$$\psi_x = - \int_0^\infty dy \sqrt{y} \frac{\psi_y v_{x,y}^s}{2E_y} \tanh\left(\frac{E_y}{2\tau}\right). \quad (\text{B11})$$

In a bulk 3-dimensional sample the macroscopic charge has the effect of maintaining the number of electrons inside the sample constant. Consequently the chemical potential is temperature dependent, which can be observed experimentally as a temperature dependence of the workfunction [27]. To account for this effect, the condition (B2) must be applied simultaneously with the solution of the gap equation. Since the shift of chemical potential is of order  $\Delta^2/4\varepsilon_F$ , the effect becomes relevant in superconductors where  $\Delta$  is of comparable size as  $\varepsilon_F$  which, given the hierarchy of energy scales shown in Fig. 2, clearly doesn't apply to the system considered here. For this reason it makes no significant difference if the gap equation is solved in the canonical ensemble or in the grand canonical ensemble. Here we follow the latter approach and fix the chemical potential at  $\mu = \varepsilon_F$ .

The entropy is

$$S(T) = -\frac{dw}{d\tau} k_B = \frac{3}{2} k_B \int_0^\infty dx \sqrt{x} \left[ \frac{\ln(1 + e^{E_x/\tau})}{1 + e^{E_x/\tau}} + \frac{\ln(1 + e^{-E_x/\tau})}{1 + e^{-E_x/\tau}} \right] \quad (\text{B12})$$

The specific heat is obtained by (numerical) differentiation of  $S(T)$

$$C(T) = T \frac{d}{dT} S(T) \quad (\text{B13})$$

In Fig. 6 entropy, specific heat and order parameter at the Fermi surface are displayed as a function of temperature for the case  $r_s = 2.08$ .

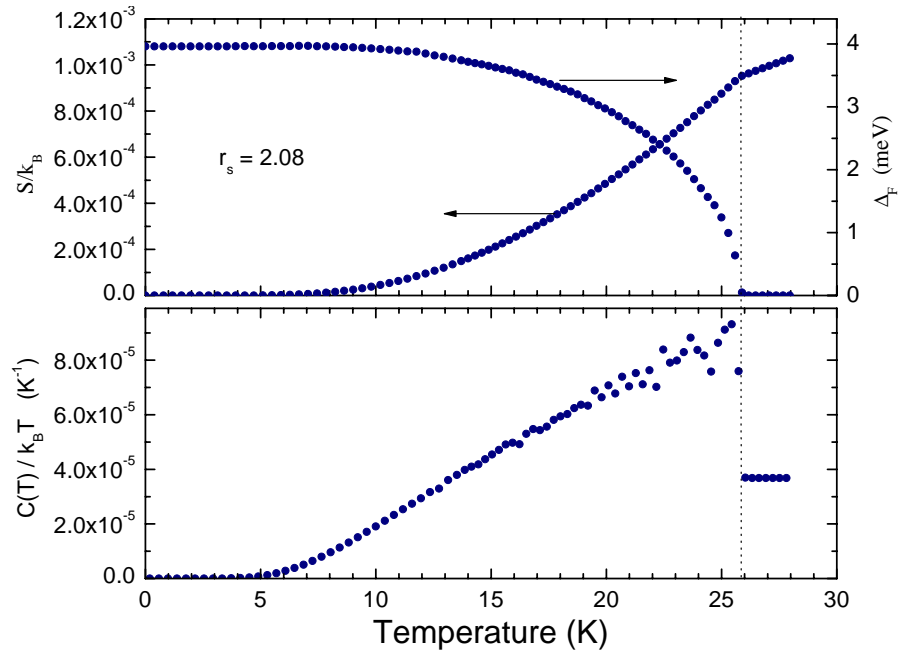


Figure 6. Temperature dependence of the order parameter at the Fermi surface, the entropy and the specific heat for  $r_s = 2.08$  in the case of hydrogen ( $m_N = m_p$ ) calculated with the trapezoidal rule (“Numerical implementation” in Methods). The noise of  $C(T)/T$  in the lower panel is stronger than that of the entropy, because it was calculated taking the numerical derivative of  $S(T)$ .

### Appendix C: Numerical implementation

It is easy to demonstrate that at  $T_c$  the gap function is real, apart from an arbitrary phase that doesn't depend on  $k$  and that we can set to zero. It is in principle possible that at an additional transition takes place to a state with a  $k$ -dependent phase. Since this requires a finite amplitude of the order parameter, it can only happen at a temperature lower than  $T_c$  so that it wouldn't influence  $T_c$ . Since our purpose is to determine  $T_c$ , we can limit the present discussion to a real-valued order parameter. In this case the expression of the grand potential formulated for numerical coding is :

$$w = \frac{3}{4} \sum_h \left[ -2\tau \ln \left( 1 + e^{-X_h/\tau} \right) + \xi_h - X_h + \frac{\psi_h(2\psi_h - \phi_h)}{2X_h} \tanh(X_h/2\tau) \right] D_h \quad (C1)$$

where

$$\xi_h = x_h - 1 \quad (C2)$$

$$X_h = \sqrt{\xi_h^2 + \psi_h^2} \quad (C3)$$

$$D_h = \sqrt{x_h} dx_h \quad (C4)$$

$$\phi_h(n) = - \sum_{j=1}^N \left[ \frac{\psi_j(n) \tanh(X_j/2\tau) v^s(x_h, x_j)}{2X_j} \right] D_j - \left[ \frac{\psi_N(n) \tanh(X_N/2\tau) v^s(x_h, x_N)}{2X_N} \right] \times \frac{2}{3} x_N^{3/2} \quad (C5)$$

The second term on the right hand side is the analytical integral in the interval  $\{x_N; \infty\}$ , taking into account that for  $x_j \gg 1$  both  $v^s(x_i, x_j) \propto x_j^{-1}$  and  $\psi_j(n) \propto x_j^{-1}$ . For  $x_j \gg 1$  we can use  $X_j \approx x_j$ . Consequently the integrand is proportional to  $x_j^{-5/2}$ , from which follows the second term. The first and second derivatives of the grand potential are

$$\frac{dw}{d\psi_i} = \frac{3}{4} \left[ \frac{\xi_i^2 \tanh(X_i/2\tau)}{X_i^3} + \frac{\psi_i^2}{2\tau X_i^2 \cosh^2(X_i/2\tau)} \right] [\psi_i - \phi_i] D_i \quad (C6)$$

$$\begin{aligned} \frac{\partial^2 w}{\partial \psi_i^2} &= \frac{3}{4} \frac{\psi_i}{X_i^3} \left[ \frac{3\xi_i^2 + \psi_i^2}{2\tau X_i^2 \cosh^2(X_i/2\tau)} - \frac{\psi_i^2 \tanh(X_i/2\tau)}{4\tau^2 \cosh^2(X_i/2\tau)} - \frac{3\xi_i^2 \tanh(X_i/2\tau)}{X_i^2} \right] [\psi_i - \phi_i] \delta_{i,m} D_i + \\ &+ \frac{3}{4} \frac{1}{X_i^2} \left[ \frac{\xi_i^2 \tanh(X_i/2\tau)}{X_i} + \frac{\psi_i^2}{2\tau \cosh^2(X_i/2\tau)} \right] D_i + \\ &+ \frac{3}{8} \frac{v^s(x_i, x_i)}{X_i^2 X_i^2} \left[ \frac{\xi_i^2 \tanh(X_i/2\tau)}{X_i} + \frac{\psi_i^2}{2\tau \cosh^2(X_i/2\tau)} \right] \left[ \frac{x_i^2 \tanh(X_i/2\tau)}{X_i} + \frac{\psi_i^2}{2\tau \cosh^2(X_i/2\tau)} \right] D_i^2 \end{aligned} \quad (C7)$$

At the minimum we have  $dw/d\psi_i = 0$  for all  $\psi_i$ . We search for the minimum using the steepest descent method, *i.e.*, we iterate

$$\psi_i(n+1) = \psi_i(n) - \frac{\eta}{2} \frac{\partial w(n)/\partial \psi_i(n)}{\partial^2 w(n)/\partial \psi_i(n)^2} \quad (C8)$$

where  $\eta < 1$  to ensure convergence of the iteration. The first step consisted of solving the equation for  $r_s = 50$ , and this process was repeated down to  $r_s = 0.5$  using the output for  $\psi_i$  as the starting values for each subsequent  $r_s$  value. For the calculation of the temperature dependence, for each  $r_s$  value the temperature was increased from 0

Energy interval	No. of equidistant energy values
$-1.0 < \xi_j < 0.1$	$n$
$-0.1 < \xi_j < -4\sqrt{\psi_F^2 + \tau^2}$	$4n$
$-4\sqrt{\psi_F^2 + \tau^2} < \xi_j < 4\sqrt{\psi_F^2 + \tau^2}$	$n$
$4\sqrt{\psi_F^2 + \tau^2} < \xi_j < 0.1$	$4n$
$0.1 < \xi_j < 1$	$n$
$1 < \xi_j < 100$	$n$
$100 < \xi_j < 10^4$	$n$
$10^4 < \xi_j < \infty$	analytical continuation

Table I. **Discretization of the energy axis** used in numerical integrals.



to  $0.85\psi_F$  where  $\psi_F$  is the order parameter at  $\varepsilon_F$ , using the output for  $\psi_i$  as the starting values for each subsequent temperature. Integrations were done using the trapezium method. The energy mesh used is specified in the Table I. In each new iteration  $\psi_F$  is taken to be the output value of previous iteration. Consequently, if the order parameter converges to a small value the set of energy values is adjusted correspondingly to a finer mesh around  $\varepsilon_F$ . Numerical verification indicates that  $n = 500$  is sufficiently large, giving a grand total of 6500 energy points at which the order parameter needs to be calculated self-consistently.

Although integrals over a log-divergence are convergent, jitter is unavoidable in the present iterative procedure due to finite sampling of the energy axis. To dampen the jitter we replace in Eq. 4

$$\ln \left| \frac{4z^2 - (\sqrt{x} - \sqrt{y})^2 [4z_0^2 - z^2\gamma^{-2}]}{4z^2 - (\sqrt{x} + \sqrt{y})^2 [4z_0^2 - z^2\gamma^{-2}]} \right| \quad \text{with} \quad \ln \left| \frac{4(z^2 + i\delta^2) - (\sqrt{x} - \sqrt{y})^2 [4z_0^2 - z^2\gamma^{-2}]}{4(z^2 + i\delta^2) - (\sqrt{x} + \sqrt{y})^2 [4z_0^2 - z^2\gamma^{-2}]} \right| \quad (\text{C9})$$

where  $\delta = 2/n$ . At equilibrium the grand potential becomes

$$w = \frac{3}{4} \int_0^\infty dx \sqrt{x} \left[ -2\tau \ln \left( 1 + e^{-E_x/\tau} \right) + \xi_x - E_x + \frac{\psi_x^2}{2E_x} \tanh \left( \frac{E_x}{2\tau} \right) \right] \quad (\text{C10})$$

where  $\psi_x$  is order parameter at the free energy minimum. For the purpose of displaying the energy dependence we choose the sign of  $\psi_x$  to be positive at the Fermi surface. The condensation energy is the energy saving at  $T = 0$  of the superconducting state compared to the trivial ( $\psi = 0$ ) solution of the gap-equation:

$$e_c = w_0^{(n)} - w_0^{(sc)} \quad (\text{C11})$$

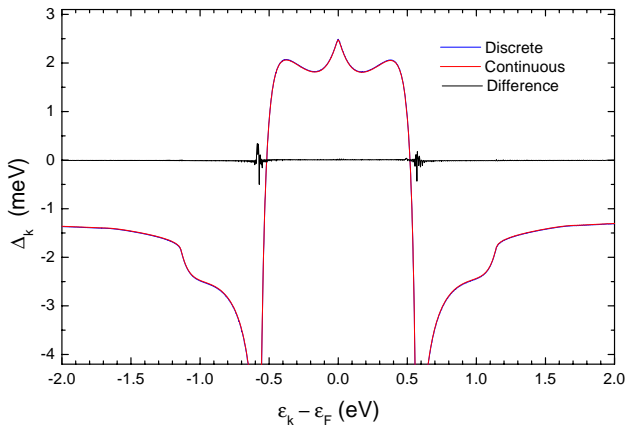


Figure 7. Difference of the gap-function at  $T = 0$  calculated with two different numerical codes shown in Fig. 3.  $\Delta(\varepsilon) = \Delta_{cont}(\varepsilon) - \Delta_{discr}(\varepsilon)$ , where the integrals in the numerical code for  $\Delta_{discr}(\varepsilon)$  are calculated with the trapezoidal rule (Appendix C), and those for  $\Delta_{cont}(\varepsilon)$  with a piecewise-continuous function of  $x$  (Appendix D).

#### Appendix D: Solution without discretization

The interaction  $v_{x,y}^s$  entering the gap equation (B11) presents logarithmic singularities. This may lead to inaccuracies when the integral is evaluated using a trapezoidal rule. We have investigated this issue by means of an alternative approach, where the gap function  $\psi_x$  is represented as a piecewise-continuous function of  $x$ . In each piece, beside polynomials of arbitrary order, we use a variety of functions to capture the precise behavior of  $\psi_x$ , including logarithms and power laws.  $\psi_y$  being a continuous function, the integral can be split at the singularities of  $v_{x,y}^s$  and evaluated to the desired accuracy using Gaussian quadratures, without discretization error. At each iteration towards self-consistency, we fit our set of functions to  $\psi_x$  in sub-domains that are recursively split until a satisfactory fit is found. This method is much slower, but produces results that are hardly distinguishable from those obtained by discretizing the integral (see Fig. 3). In Fig. 7 the difference of the two results is displayed. The differences are small, and most pronounced near the singularities. We conclude that our results are not significantly affected by discretization errors.

- 
- [1] J. Bardeen, L. N. Cooper, and J. R. Schrieffer, “Theory of Superconductivity,” *Phys. Rev.* **108**, 1175 (1957).
  - [2] P. G. De Gennes, *Superconductivity of Metals and Alloys* (Benjamin, New York, Amsterdam, 1966).
  - [3] N. W. Ashcroft, “Metallic Hydrogen: A High-Temperature Superconductor?” *Phys. Rev. Lett.* **21**, 1748 (1968).
  - [4] C. F. Richardson and N. W. Ashcroft, “High Temperature Superconductivity in Metallic Hydrogen: Electron-Electron Enhancements,” *Phys. Rev. Lett.* **78**, 118 (1997).
  - [5] T. W. III Barbee, Alberto Garcia, and M. L. Cohen, “First-principles prediction of high-temperature superconductivity in metallic hydrogen,” *Nature* **340**, 369 (1989).
  - [6] N. W. Ashcroft, “Hydrogen Dominant Metallic Alloys: High Temperature Superconductors?” *Phys. Rev. Lett.* **92**, 187002 (2004).

- [7] V. L. Ginzburg and D. A. Kirzhnits, “Superconductivity in White Dwarfs and Pulsars,” *Nature* **220**, 148 (1968).
- [8] D. A. Kirzhnits, “Superconductivity in Systems with Arbitrary Interaction Sign,” *ZhETF Pis. Red.* **9**, 360 (1969).
- [9] L. Boeri, R. Hennig, P. Hirschfeld, G. Profeta, A. Sanna, E. Zurek, W. E. Pickett, M. Amsler, R. P. Dias, M. I. Eremets, C. Heil, R. J. Hemley, H. Liu, Y. Ma, C. Pierleoni, A. N. Kolmogorov, R. Rybin, D. Novoselov, V. Anisimov, A. R. Oganov, C. J. Pickard, T. Bi, R. Arita, I. Errea, C. Pellegrini, R. Requist, E. K. U. Gross, E. R. Margine, S. R. Xie, Y. Quan, A. Hire, L. Fanfarillo, G. R. Stewart, J. J. Hamlin, V. Stanev, R. S. Gonnelli, E. Piatti, D. Romanin, D. Daghero, and R. Valenti, “The 2021 room-temperature superconductivity roadmap,” *Journal of Physics: Condensed Matter* **34**, 183002 (2022).
- [10] D. Garisto, “Exclusive: official investigation reveals how superconductivity physicist faked blockbuster results,” *Nature* (2024), 10.1038/d41586-024-00976-y.
- [11] R.T. Howie, P. Dalladay-Simpson, and E. Gregoryanz, “Raman spectroscopy of hot hydrogen above 200 GPa,” *Nature Mater* **14**, 495 (2015).
- [12] M. Eremets and I. Troyan, “Conductive dense hydrogen,” *Nature Mater* **10**, 927 (2011).
- [13] Ho-kwang Mao and Russell J. Hemley, “Ultrahigh-pressure transitions in solid hydrogen,” *Rev. Mod. Phys.* **66**, 671 (1994).
- [14] J. Dewar, “Sur la solidification de l’hydrogene,” *Annales de Chimie et de Physique* **18**, 145 (1899).
- [15] J. E. Jaffe and N. W. Ashcroft, “Superconductivity in liquid metallic hydrogen,” *Phys. Rev. B* **23**, 6176 (1981).
- [16] J. Jaffe and N. W. Ashcroft, “Critical fields of liquid superconducting metallic hydrogen,” *Phys. Rev. B* **27**, 5852 (1983).
- [17] K. Mouloupoulos and N. W. Ashcroft, “Generalized Coulomb pairing in the condensed state,” *Phys. Rev. Lett.* **66**, 2915 (1991).
- [18] E. Babaev, A. Sudbo, and N. W. Ashcroft, “A superconductor to superfluid phase transition in liquid metallic hydrogen,” *Nature* **431**, 666 (2004).
- [19] Leon N. Cooper, “Bound Electron Pairs in a Degenerate Fermi Gas,” *Phys. Rev.* **104**, 1189 (1956).
- [20] G. M. Eliashberg, “Interactions between electrons and lattice vibrations in a superconductor,” *Sov. Phys. JETP* **11** (1960).
- [21] I. I. Mazin and R. E. Cohen, “Insulator-metal transition in solid hydrogen: Implication of electronic-structure calculations for recent experiments,” *Phys. Rev. B* **52**, R8597 (1995).
- [22] J. E. Hirsch, *Superconductivity begins with H: both properly understood, and misunderstood: Superconductivity basics rethought* (World Scientific, 2020).
- [23] H. Alfvén, “Existence of Electromagnetic-Hydrodynamic Waves,” *Nature* **150**, 405 (1942).
- [24] David R. Williams, “Jupiter Fact Sheet,” *NASA* (2021).
- [25] D. L. Kaplan, J. Boyles, B. H. Dunlap, S. P. Tendulkar, A. T. Deller, S. M. Ransom, M. A. McLaughlin, D. R. Lorimer, and I. H. Stairs, “A 1.05 M companion to PSR J2222-0137: The coolest known white dwarf ? ,” *The Astrophysical Journal* **789** (2014), 10.1088/0004-637X/789/2/119.
- [26] G. Rickayzen, *Theory of Superconductivity* (Interscience Publishers, 1965).
- [27] G. Rietveld, N. Y. Chen, and D. van der Marel, “Anomalous temperature dependence of the work function in  $\text{YBa}_2\text{Cu}_3\text{O}_{7-\delta}$ ,” *Phys. Rev. Lett.* **69**, 2578 (1992).